



HAL
open science

Adaptive mesh refinement on Cartesian meshes applied to the mixed finite element discretization of the multigroup neutron diffusion equations

Jr. Ciarlet P, Minh-Hieu Do, François Madiot

► To cite this version:

Jr. Ciarlet P, Minh-Hieu Do, François Madiot. Adaptive mesh refinement on Cartesian meshes applied to the mixed finite element discretization of the multigroup neutron diffusion equations. 2025. cea-04929216

HAL Id: cea-04929216

<https://cea.hal.science/cea-04929216v1>

Preprint submitted on 4 Feb 2025

HAL is a multi-disciplinary open access archive for the deposit and dissemination of scientific research documents, whether they are published or not. The documents may come from teaching and research institutions in France or abroad, or from public or private research centers.

L'archive ouverte pluridisciplinaire **HAL**, est destinée au dépôt et à la diffusion de documents scientifiques de niveau recherche, publiés ou non, émanant des établissements d'enseignement et de recherche français ou étrangers, des laboratoires publics ou privés.

Adaptive mesh refinement on Cartesian meshes applied to the mixed finite element discretization of the multigroup neutron diffusion equations

Patrick Ciarlet ^{*} ¹, Minh-Hieu Do ^{†2}, and François Madiot ^{‡2}

¹POEMS, CNRS, INRIA, ENSTA Paris, Institut Polytechnique de Paris, 91120 Palaiseau, France.

²Université Paris-Saclay, CEA, Service d'Études des Réacteurs et de Mathématiques Appliquées, 91191, Gif-sur-Yvette, France.

Abstract

The multigroup neutron diffusion equations are often used to model the neutron density at the nuclear reactor core scale. Classically, these equations can be recast in a mixed variational form. This chapter presents an adaptive mesh refinement approach based on *a posteriori* estimators. We focus on refinement strategies on Cartesian meshes, since such structures are common for nuclear reactor core applications.

This preprint corresponds to the Chapter 19 of volume 60 in AAMS, Advances in Applied Mechanics (to appear).

1 Introduction

In neutronics, one is interested in modelling the neutron density inside a reactor core. The neutron flux density in the reactor core is determined by solving the transport equation which depends on seven variables: space (3), direction (2), energy or modulus of the velocity (1), and time (1). Due to the high dimensionality of the problem, the numerical resolution of this equation faces some challenges in terms of computational cost. In practice, the neutron flux density can be modeled by the diffusion equations at the reactor core scale.

Achieving an accurate and efficient resolution of the discretization is challenging. Adaptive Mesh Refinement (AMR) strategies have emerged in the late seventies to tackle this crucial aspect. The objective is to reach a target accuracy, on the solution or on a functional output, at an optimal computational cost. In fact, AMR strategies can be categorized: *h*-refinement (mesh subdivision) [29]; *p*-refinement (local increase of the order of approximation) [3]; or *r*-refinement (moving mesh) [6]. The above strategies can be mixed together, such as *hp*-refinement [2, 11] and *hr*-refinement [20]. In neutronics, we are typically in the case of heterogeneous coefficients which may induce some singularities in the solution of the problems at hand, that is a loss of regularity of

^{*}patrick.ciarlet@ensta-paris.fr

[†]minh-hieu.do@cea.fr

[‡]francois.madiot@cea.fr

the solution due to the discontinuities in the data. For this reason, we focus on the mesh subdivision strategy, which is the most suitable solution to address this kind of difficulty.

Adaptive mesh refinement is based on an essential ingredient: *a posteriori* estimates. In neutronics, *a posteriori* error control is an ongoing research topic. AMR based on *a posteriori* estimators for the transport equation have been studied in [16, 17, 21, 22, 25]. In [16, Section 3.3], the authors address the issue of the regularity assumption used for the *a posteriori* estimate. In [21, 22, 25], the *a posteriori* estimates are based on the Dual Weighted Residual method where the guaranteed estimator involves an exact adjoint solution. In [17], they devise a reliable estimate that relies on the definition of a dual problem and highlight a lack of efficiency due to the absence of stability in this dual problem. Rigorous estimates that do not require excess regularity, together with an adaptive mesh refinement strategy, have been proposed for the resolution of the source problem on the transport equation [9]. Following this work, theoretical aspects on the eigenvalue problem has been addressed in [10]. In these papers, the authors devise a numerical strategy relying on accuracy controlled operator evaluation, such as in [9] for the resolution of the source problem.

At the reactor core scale, using simplified models is common in the nuclear industry. Precisely, the simplified models can be the neutron diffusion model or the simplified transport model. In [7], we derive rigorous *a posteriori* error estimates for mixed finite element discretizations of the Neutron Diffusion equations, and propose an adaptive mesh refinement strategy that preserves the Cartesian structure. A first application of this approach to the criticality problem was performed in [13] albeit with subefficient estimators. Regarding the industrial context and specifically the numerical simulations, our approach is part of the development of a mixed finite element solver called MINOS [4] in the APOLLO3[®] code [23].

The outline of this chapter is as follows. Section 2 introduces some notations. Section 3 describes the physical model, the variational formulation and its discretization. Section 4 gives some algorithmic motivations related to the MINOS solver [4]. Section 5 details *a posteriori* error estimates. Section 6 includes the algorithm of our Adaptive Mesh Refinement (AMR) approach. Section 7 illustrates numerically our AMR strategy.

2 Notations

We choose the same notations as in [7]. Throughout the paper, C is used to denote a generic positive constant which is independent of the mesh size, the mesh and the quantities/fields of interest. We also use the shorthand notation $A \lesssim B$ for the inequality $A \leq CB$, where A and B are two scalar quantities, and C is a generic constant.

Vector-valued (resp. tensor-valued) function spaces are written in boldface character (resp. blackboard characters); for the latter, the index *sym* indicates symmetric fields. Given an open set $\mathcal{O} \subset \mathbb{R}^d$, $d = 1, 2, 3$, we use the notation $(\cdot, \cdot)_{0, \mathcal{O}}$ (respectively $\|\cdot\|_{0, \mathcal{O}}$) for the $L^2(\mathcal{O})$ and $\mathbf{L}^2(\mathcal{O}) = (L^2(\mathcal{O}))^d$ inner products (resp. norms).

When the boundary $\partial\mathcal{O}$ is Lipschitz, \mathbf{n} denotes the unit outward normal vector field to $\partial\mathcal{O}$. Finally, it is assumed that the reader is familiar with vector-valued function spaces related to the diffusion equation, such as $\mathbf{H}(\text{div}; \mathcal{O})$, $\mathbf{H}_0(\text{div}; \mathcal{O})$ etc.

Let $G \in \mathbb{N} \setminus \{0, 1\}$. Given a function space W , we denote by \underline{W} the product space W^G . We extend the notation $(\cdot, \cdot)_{0, \mathcal{O}}$ (respectively $\|\cdot\|_{0, \mathcal{O}}$) to the $\underline{L}^2(\mathcal{O})$ and $\underline{\mathbf{L}}^2(\mathcal{O})$ inner products (resp. norms). Specifically, we let Ω be a bounded, connected and open subset of \mathbb{R}^d for $d = 2, 3$, having a Lipschitz boundary which is piecewise smooth. We split Ω into N open, connected, disjoint parts $\{\Omega_i\}_{1 \leq i \leq N}$ with Lipschitz, piecewise smooth boundaries $\bar{\Omega} = \cup_{1 \leq i \leq N} \bar{\Omega}_i$: the set $\{\Omega_i\}_{1 \leq i \leq N}$ is called a partition

of Ω . For a field v defined over Ω , we shall use the notations $v_i = v|_{\Omega_i}$, for $1 \leq i \leq N$. Given the partition $\{\Omega_i\}_{1 \leq i \leq N}$ of Ω , we introduce a function space with piecewise regular elements:

$$\mathcal{P}W^{1,\infty}(\Omega) = \{D \in L^\infty(\Omega) \mid D_i \in W^{1,\infty}(\Omega_i), 1 \leq i \leq N\}.$$

To measure $\psi \in \mathcal{P}W^{1,\infty}(\Omega)$, we use the natural norm $\|\psi\|_{\mathcal{P}W^{1,\infty}(\Omega)} = \max_{i=1,N} \|\psi_i\|_{W^{1,\infty}(\Omega_i)}$.

3 The neutron diffusion model

The neutron flux density in the reactor core is determined by solving the transport equation which depends on seven variables: space (3), direction (2), energy or modulus of the velocity (1), and time (1). It physically states the balance between, on the one hand, the emission of neutrons by fission and, on the other hand, the absorption, scattering, and leakage (at the boundaries) of neutrons. The most common discretization of the energy variable is the multigroup approximation where the energy domain is divided into subintervals called energy groups. In practice, the neutron flux density is usually modeled by the multigroup diffusion equations [14, Chapter 7] at the reactor core scale.

In many practical situations, only a steady-state solution is relevant and it requires to solve a generalized eigenvalue problem. In the companion paper [13], we perform adaptive mesh refinement for the multigroup diffusion case on this so-called criticality problem. We present in this section some theoretical results underlying this approach on a source problem. For $G \geq 2$, we let $\mathcal{I}_G := \{1, \dots, G\}$ be the set of energy groups.

Let $\mathbf{q} := (q_x^g)_{x=1,d}^{g=1,G}$, $\mathbf{q}^g = (q_x^g)_{x=1,d} \in \mathbb{R}^d$ for $1 \leq g \leq G$, and $\text{div } \mathbf{q} = (\text{div } \mathbf{x}\mathbf{q}^g)^{g=1,G} \in \mathbb{R}^G$.

Let \mathbb{T}_e be the even removal matrix. At (almost) every point in Ω , it is a matrix of $\mathbb{R}^{G \times G}$:

$$\forall (g, g') \in \mathcal{I}_G \times \mathcal{I}_G, \quad (\mathbb{T}_e)_{g,g'} = \begin{cases} \Sigma_{r,0}^g := \Sigma_t^g - \Sigma_{s,0}^{g \rightarrow g} & \text{if } g = g', \\ -\Sigma_{s,0}^{g' \rightarrow g} & \text{if } g \neq g', \end{cases}$$

where $\Sigma_{s,0}^{g' \rightarrow g}$ are the Legendre moments of order 0 of the macroscopic scattering cross sections from energy group g' to energy group g and the coefficient Σ_t^g is the macroscopic total cross section of energy group g [14, Part 2, Chapter IV, Section A, p.124-127]. We emphasize that, in general, the matrix \mathbb{T}_e is not symmetric.

We denote \mathbb{D} the diffusion matrix. At (almost) every point in Ω , it is a diagonal matrix of $\mathbb{R}^{G \times G}$:

$$\forall g \in \mathcal{I}_G, \quad \mathbb{D}_{g,g} = D^g.$$

where D^g is the scalar-valued diffusion coefficient of energy group g . Mathematically speaking, the coefficients of the measurable fields of matrices \mathbb{T}_e and \mathbb{D} are supposed to be such that:

$$\left\{ \begin{array}{l} (0) \quad \forall g, g' \in \mathcal{I}_G, (D^g, \Sigma_{r,0}^g, \Sigma_{s,0}^{g' \rightarrow g}) \in \mathcal{P}W^{1,\infty}(\Omega) \times \mathcal{P}W^{1,\infty}(\Omega) \times L^\infty(\Omega), \\ (i) \quad \exists (D)_*, (D)^* > 0, \forall g \in \mathcal{I}_G, (D)_* \leq D^g \leq (D)^* \text{ a.e. in } \Omega, \\ (ii) \quad \exists (\Sigma_{r,0})_*, (\Sigma_{r,0})^* > 0, \forall g \in \mathcal{I}_G, (\Sigma_{r,0})_* \leq \Sigma_{r,0}^g \leq (\Sigma_{r,0})^* \text{ a.e. in } \Omega, \\ (iii) \quad \exists \epsilon \in (0, (G-1)^{-1}), \forall g, g' \in \mathcal{I}_G, g' \neq g, |\Sigma_{s,0}^{g \rightarrow g'}| \leq \epsilon \Sigma_{r,0}^g \text{ a.e. in } \Omega. \end{array} \right. \quad (1)$$

As a consequence of (1): the matrix \mathbb{T}_e is (almost everywhere) strictly diagonally dominant (so it is invertible); the matrix \mathbb{D} is also invertible (almost everywhere).

Remark 3.1. Hypothesis (1)–(iii) models accurately the core of a pressurized water reactor and, in this case, ϵ is usually a small fraction of $(G - 1)^{-1}$. We refer to Appendix A for an illustration. So on every row of \mathbb{T}_e , the off-diagonal entries are much smaller than the diagonal entries. In particular, the inverse of \mathbb{T}_e is well-approximated by the inverse of its diagonal.

Remark 3.2. In the absence of up-scattering, i.e. in the situation where for all $1 \leq g < g' \leq G$ $\Sigma_{s,0}^{g' \rightarrow g} = 0$, the matrix \mathbb{T}_e is lower triangular by (energy group) block.

We consider the following multigroup neutron diffusion equations, with vanishing Dirichlet boundary condition, also denoted zero-flux boundary condition. The criticality problem (in its primal form) writes

$$\begin{cases} \text{Find } (\phi, k_{\text{eff}}) \in (\underline{H}_0^1(\Omega) \setminus \{0\}) \times \mathbb{R} \text{ such that} \\ k_{\text{eff}} \text{ is an eigenvalue with maximal modulus, and} \\ -\text{div}(\mathbb{D} \mathbf{grad} \phi) + \mathbb{T}_e \phi = \frac{1}{k_{\text{eff}}} M_f \phi \text{ in } \Omega, \end{cases} \quad (2)$$

where $M_f \in (\mathbb{R})^{G \times G}$ is the fission matrix defined for all $(g, g') \in \mathcal{I}_G \times \mathcal{I}_G$ by

$$(M_f)_{g,g'} = \chi^g (\nu \Sigma_f)^{g'},$$

where χ^g is the total spectrum of energy group g , $\nu^{g'}$ is the average number of neutrons emitted by fission of energy group g' and $\Sigma_f^{g'}$ is the macroscopic fission cross section of energy group g' . The coefficients of the fission matrix are assumed to be such that

$$\begin{cases} \forall g \in \mathcal{I}_g, ((\nu \Sigma_f)^g, \chi^g) \in L^\infty(\Omega) \times L^\infty(\Omega), \\ \forall g \in \mathcal{I}_g, 0 \leq (\nu \Sigma_f)^g \text{ a.e. in } \Omega, \text{ and } \underline{(\nu \Sigma_f)} \neq 0 \text{ a.e. in } \Omega. \end{cases} \quad (3)$$

Under the assumptions (1) and (3) on the coefficients, the eigenvalue k_{eff} with the greatest modulus is simple, real and strictly positive (see [12, Chapter XXI]). Furthermore, the associated eigenfunction ϕ is real and positive a.e. in Ω , up to a multiplicative constant. In neutronics, ϕ and k_{eff} are respectively called the neutron flux and the effective multiplication factor. The physical state of the core reactor is characterized by the effective multiplication factor: if $k_{\text{eff}} = 1$: the nuclear chain reaction is self-sustaining; if $k_{\text{eff}} > 1$: the chain reaction is diverging; if $k_{\text{eff}} < 1$: the chain reaction vanishes.

Given a source term $S_f \in \underline{L}^2(\Omega)$, the source problem writes,

$$\begin{cases} \text{Find } \phi \in \underline{H}_0^1(\Omega) \text{ such that} \\ -\text{div}(\mathbb{D} \mathbf{grad} \phi) + \mathbb{T}_e \phi = S_f \text{ in } \Omega. \end{cases} \quad (4)$$

Under the assumptions (1) on the coefficients, the primal problem (4) is well-posed, in the sense that for all $S_f \in \underline{L}^2(\Omega)$, there exists one and only one solution $\phi \in \underline{H}_0^1(\Omega)$ that solves (4), with the bound $\|\phi\|_{1,\Omega} \lesssim \|S_f\|_{0,\Omega}$. Provided that the coefficients D^g , for $1 \leq g \leq G$, are piecewise smooth, the solution has extra smoothness (see eg. Proposition 1 in [8] in the monogroup case). Instead of imposing a Dirichlet boundary condition on $\partial\Omega$, one can consider a Neumann or Fourier boundary condition $\mu_F^g \phi^g + (D^g \mathbf{grad} \phi^g) \cdot \mathbf{n} = 0$, with $\mu_F^g \geq 0$ for all $1 \leq g \leq G$. Results are similar. In neutronics, the homogeneous Neumann boundary condition is called reflective boundary condition, while the Fourier boundary condition with $\mu_F^g = 1/2$ is denoted vacuum boundary condition.

3.1 Mixed variational formulation

Let us introduce the function spaces:

$$\begin{aligned}\mathcal{H} &= \{ \xi = (\mathbf{q}, \psi) \in \underline{\mathbf{L}}^2(\Omega) \times \underline{L}^2(\Omega) \}, \quad \|\xi\|_{\mathcal{H}} = \left(\|\mathbf{q}\|_{0,\Omega}^2 + \|\psi\|_{0,\Omega}^2 \right)^{1/2}; \\ \mathcal{X} &= \{ \xi = (\mathbf{q}, \psi) \in \underline{\mathbf{H}}(\text{div}, \Omega) \times \underline{L}^2(\Omega) \}, \quad \|\xi\|_{\mathcal{X}} = \left(\|\mathbf{q}\|_{\underline{\mathbf{H}}(\text{div}, \Omega)}^2 + \|\psi\|_{0,\Omega}^2 \right)^{1/2}.\end{aligned}$$

From now on, we use the notations: $\zeta = (\mathbf{p}, \phi)$ and $\xi = (\mathbf{q}, \psi)$.

The solution ϕ to (4) belongs to $\underline{H}^1(\Omega)$, so if one lets $\mathbf{p} = -\mathbb{D} \mathbf{grad} \phi \in \underline{\mathbf{L}}^2(\Omega)$, the multigroup neutron diffusion source problem may be written as:

$$\begin{cases} \text{Find } (\mathbf{p}, \phi) \in \underline{\mathbf{H}}(\text{div}, \Omega) \times \underline{H}_0^1(\Omega) \text{ such that} \\ -\mathbb{D}^{-1} \mathbf{p} - \mathbf{grad} \phi = 0 \text{ in } \Omega, \\ \text{div } \mathbf{p} + \mathbb{T}_e \phi = S_f \text{ in } \Omega. \end{cases} \quad (5)$$

Solving the mixed problem (5) is equivalent to solving (4). The variational formulation for the mixed problem associated to problem (5) writes

$$\begin{cases} \text{Find } (\mathbf{p}, \phi) \in \underline{\mathbf{H}}(\text{div}, \Omega) \times \underline{L}^2(\Omega) \text{ such that} \\ \forall (\mathbf{q}, \psi) \in \underline{\mathbf{H}}(\text{div}, \Omega) \times \underline{L}^2(\Omega), \quad c((\mathbf{p}, \phi), (\mathbf{q}, \psi)) = (S_f, \psi)_{0,\Omega}, \end{cases} \quad (6)$$

where the bilinear form c is defined as

$$c : ((\mathbf{p}, \phi), (\mathbf{q}, \psi)) \mapsto -(\mathbb{D}^{-1} \mathbf{p}, \mathbf{q})_{0,\Omega} + (\phi, \text{div } \mathbf{q})_{0,\Omega} + (\psi, \text{div } \mathbf{p})_{0,\Omega} + (\mathbb{T}_e \phi, \psi)_{0,\Omega}. \quad (7)$$

Note that \mathbb{D}^{-1} is a measurable field of diagonal matrices, which positive diagonal entries that are uniformly bounded away from 0. Hence, the form c is continuous, bilinear and symmetric on $\underline{\mathbf{H}}(\text{div}, \Omega) \times \underline{L}^2(\Omega)$, and one may prove that the mixed formulation (6) is well-posed, see theorem 3.16 in [18]. As a matter of fact, the result is obtained by proving an inf-sup condition in $\mathcal{X} = \underline{\mathbf{H}}(\text{div}, \Omega) \times \underline{L}^2(\Omega)$, which we recall here.

Theorem 3.1. *Let \mathbb{D} and \mathbb{T}_e satisfy (1). Then, the bilinear symmetric form c fulfills an inf-sup condition:*

$$\exists \eta > 0, \quad \inf_{\zeta \in \mathcal{X}} \sup_{\xi \in \mathcal{X}} \frac{c(\zeta, \xi)}{\|\zeta\|_{\mathcal{X}} \|\xi\|_{\mathcal{X}}} \geq \eta. \quad (8)$$

Similarly, the multigroup neutron diffusion criticality problem may be written as:

$$\begin{cases} \text{Find } (\mathbf{p}, \phi, k_{\text{eff}}) \in \underline{\mathbf{H}}(\text{div}, \Omega) \times (\underline{H}_0^1(\Omega) \setminus \{0\}) \times \mathbb{R} \text{ such that} \\ k_{\text{eff}} \text{ is an eigenvalue with maximal modulus, and} \\ -\mathbb{D}^{-1} \mathbf{p} - \mathbf{grad} \phi = 0 \text{ in } \Omega, \\ \text{div } \mathbf{p} + \mathbb{T}_e \phi = \frac{1}{k_{\text{eff}}} M_f \phi \text{ in } \Omega. \end{cases} \quad (9)$$

The variational formulation for the mixed problem associated to problem (9) writes

$$\begin{cases} \text{Find } (\mathbf{p}, \phi, k_{\text{eff}}) \in \underline{\mathbf{H}}(\text{div}, \Omega) \times (\underline{L}^2(\Omega) \setminus \{0\}) \times \mathbb{R} \text{ such that} \\ k_{\text{eff}} \text{ is an eigenvalue with maximal modulus, and} \\ \forall (\mathbf{q}, \psi) \in \underline{\mathbf{H}}(\text{div}, \Omega) \times \underline{L}^2(\Omega), \quad c((\mathbf{p}, \phi), (\mathbf{q}, \psi)) = \frac{1}{k_{\text{eff}}} (M_f \phi, \psi)_{0,\Omega}. \end{cases} \quad (10)$$

3.2 Discretization

We consider conforming discretizations of (6). Let $(\mathcal{T}_h)_h$ be a family of meshes, made for instance of simplices, or of rectangles ($d = 2$), resp. cuboids ($d = 3$), indexed by a parameter h equal to the largest diameter of elements of a given mesh. We introduce discrete, finite-dimensional, spaces indexed by h as follows:

$$\mathbf{Q}_h \subset \mathbf{H}(\text{div}, \Omega), \text{ and } L_h \subset \underline{L}^2(\Omega).$$

The conforming mixed discretization of the variational formulation (6) is then:

$$\begin{cases} \text{Find } (\mathbf{p}_h, \phi_h) \in \mathbf{Q}_h \times L_h \text{ such that} \\ \forall (\mathbf{q}_h, \psi_h) \in \mathbf{Q}_h \times L_h, \quad c((\mathbf{p}_h, \phi_h), (\mathbf{q}_h, \psi_h)) = (S_f, \psi_h)_{0,\Omega}. \end{cases} \quad (11)$$

Similarly, the discrete counterpart of the criticality problem writes

$$\begin{cases} \text{Find } (\mathbf{p}_h, \phi_h, k_{\text{eff},h}) \in \mathbf{Q}_h \times (L_h \setminus \{0\}) \times \mathbb{R} \text{ such that} \\ k_{\text{eff},h} \text{ is an eigenvalue with maximal modulus, and} \\ \forall (\mathbf{q}_h, \psi_h) \in \mathbf{Q}_h \times L_h, \quad c((\mathbf{p}_h, \phi_h), (\mathbf{q}_h, \psi_h)) = \frac{1}{k_{\text{eff},h}} (M_f \phi_h, \psi_h)_{0,\Omega}. \end{cases} \quad (12)$$

We define:

$$\mathcal{X}_h = \{ \xi_h = (\mathbf{q}_h, \psi_h) \in \mathbf{Q}_h \times L_h \}, \text{ endowed with } \|\cdot\|_{\mathcal{X}}.$$

Remark 3.3. *At some point, the discrete spaces are considered locally, i.e.. restricted to one element of the mesh. So, one introduces the local spaces $\mathbf{Q}_h(K)$, $L_h(K)$, $\mathcal{X}_h(K)$ for every $K \in \mathcal{T}_h$.*

Explicit *a priori* error estimates may be derived, see eg. [18, Section 5.2].

In this paper, we focus on the Raviart-Thomas-Nédélec (RTN) Finite Element [24, 26].

For *simplicial meshes*, that is meshes made of simplices, the description of the finite element spaces RTN_k , where $k \geq 0$ is the order of the discretization can be found e.g. in [5]. Similarly for the scalar fields of L_h with the same order.

For *rectangular or Cartesian meshes*, a description of the Raviart-Thomas-Nédélec (RTN) finite element spaces can be found for instance in Section 4.2 of [19]. Let us detail the definition in dimension 3. Let $P(K)$ be the set of polynomials on $K \in \mathcal{T}_h$. We define the following subspace of $P(K)$,

$$\mathbb{Q}_{l,m,p}(K) = \{p(y_1, y_2, y_3) \in P(K) \mid p(y_1, y_2, y_3) = \sum_{i_1, i_2, i_3=0}^{l, m, p} \alpha_{i_1, i_2, i_3} y_1^{i_1} y_2^{i_2} y_3^{i_3}, \alpha_{i_1, i_2, i_3} \in \mathbb{R}\},$$

with $l, m, p \in \mathbb{N}$ and $\mathbb{Q}_l(K) = \mathbb{Q}_{l,l,l}(K)$. For $k \geq 0$, the definition of the RTN element of order k is

$$\text{RTN}_k(K) = [\underline{\mathbb{Q}_{k+1,k,k}(K)} \times \mathbf{0} \times \mathbf{0}] \oplus [\mathbf{0} \times \underline{\mathbb{Q}_{k,k+1,k}(K)} \times \mathbf{0}] \oplus [\mathbf{0} \times \mathbf{0} \times \underline{\mathbb{Q}_{k,k,k+1}(K)}].$$

The definitions of the finite element spaces RTN_k are then

$$\begin{aligned} \mathbf{Q}_h &= \{ \mathbf{q}_h \in \mathbf{H}(\text{div}, \Omega) \mid \forall K \in \mathcal{T}_h, \mathbf{q}_h|_K \in \text{RTN}_k(K) \}, \\ L_h &= \{ \psi_h \in \underline{L}^2(\Omega) \mid \forall K \in \mathcal{T}_h, \psi_h|_K \in \underline{\mathbb{Q}}_k(K) \}. \end{aligned}$$

4 Algorithmic motivations

In this section, we describe the algorithm of the MINOS solver [4]. Recall that in many practical situations, we are interested in solving the criticality problem (2) or (9). For this reason, we detail the algorithm associated to the resolution of the discrete variational formulation (12). The algorithm for the discrete source problem (11) follows a similar pattern.

For $1 \leq g \leq G$, we denote \mathbf{P}_h^g and Φ_h^g the vector of the degrees of freedom of \mathbf{p}_h^g and ϕ_h^g . Furthermore, the current vector \mathbf{P}_h^g is sorted by direction, $1 \leq x \leq d$. We may reformulate problem (12) in the following matrix formalism:

$$\text{Find } \left(Z_h := [\mathbf{P}_h^1 \ \Phi_h^1 \ \dots \ \mathbf{P}_h^G \ \Phi_h^G] \right)^T \neq 0, k_{\text{eff},h} \text{) such that } \mathbb{M}_h Z_h = \frac{1}{k_{\text{eff},h}} \mathbb{F}_h Z_h,$$

where $k_{\text{eff},h}$ is an eigenvalue with maximal modulus, \mathbb{M}_h and \mathbb{F}_h are (energy group) block matrices such that for all $g, g' \in \{1, \dots, G\}$

$$(\mathbb{M}_h)_{g,g'} := \begin{cases} \begin{pmatrix} -\mathbb{A}_h^{g,g} & \mathbb{B}_h \\ (\mathbb{B}_h)^T & \mathbb{T}_h^{g,g} \end{pmatrix} & \text{if } g' = g \\ \begin{pmatrix} 0 & 0 \\ 0 & \mathbb{T}_h^{g,g'} \end{pmatrix} & \text{otherwise} \end{cases} ; \quad (\mathbb{F}_h)_{g,g'} := \begin{pmatrix} 0 & 0 \\ 0 & \mathbb{F}_{\phi,h}^{g,g'} \end{pmatrix}.$$

The matrices $\mathbb{A}_h^{g,g}$, $\mathbb{T}_h^{g,g'}$, $\mathbb{F}_{\phi,h}^{g,g'}$, $1 \leq g, g' \leq G$, and \mathbb{B}_h are respectively associated to the following bilinear forms

$$\begin{aligned} a_{g,g} &: \begin{cases} \mathbf{H}(\text{div}, \Omega) \times \mathbf{H}(\text{div}, \Omega) & \rightarrow \mathbb{R} \\ (\mathbf{u}, \mathbf{v}) & \mapsto ((D^g)^{-1} \mathbf{u}, \mathbf{v})_{0,\Omega} \end{cases} ; \\ t_{g,g'} &: \begin{cases} L^2(\Omega) \times L^2(\Omega) & \rightarrow \mathbb{R} \\ (u, v) & \mapsto ((\mathbb{T}_e)_{g,g'} u, v)_{0,\Omega} \end{cases} ; \\ f_{g,g'} &: \begin{cases} L^2(\Omega) \times L^2(\Omega) & \rightarrow \mathbb{R} \\ (u, v) & \mapsto (\chi^g (\nu \Sigma_f)^{g'} u, v)_{0,\Omega} \end{cases} ; \\ b &: \begin{cases} \mathbf{H}(\text{div}, \Omega) \times L^2(\Omega) & \rightarrow \mathbb{R} \\ (\mathbf{v}, u) & \mapsto (u, \text{div } \mathbf{v})_{0,\Omega} \end{cases} . \end{aligned}$$

A standard iterative resolution strategy is the inverse power method. For each iteration, a classical strategy is to solve the linear systems with matrix \mathbb{M}_h via two nested level of iterations, the so-called outer and inner iterations. The slight difference is that we do not solve *exactly* the linear systems. Instead, we perform outer iterations as detailed below, which results in approximate solves. It is known that the convergence of the inverse power method is governed by the ratio between the first and second eigenvalue. Our resolution algorithm with approximate solves behaves similarly. In order to mitigate this effect, we apply the classical Chebyshev acceleration [28]. This acceleration is an extrapolation method based on Chebyshev polynomials. In the rest of this section, we will omit the subscript h .

4.1 Outer iteration

The outer iteration is similar to a Gauss Seidel iteration on the energy groups. It is defined as follows. Let $Z_M = [\mathbf{P}_M^1 \ \Phi_M^1 \ \cdots \ \mathbf{P}_M^G \ \Phi_M^G]^T$ and k_M be the approximation of Z and k at the outer iteration number M . For increasing $g = 1, \dots, G$, we solve the linear systems

$$(\mathbb{M})_{g,g} \begin{bmatrix} \mathbf{P}_{M+1}^g \\ \Phi_{M+1}^g \end{bmatrix} = \begin{bmatrix} S_{M,\mathbf{P}}^g \\ S_{M,\phi}^g \end{bmatrix}$$

iteratively, where

$$\begin{bmatrix} S_{M,\mathbf{P}}^g \\ S_{M,\phi}^g \end{bmatrix} = \frac{1}{k_M} \sum_{g'=1}^G (\mathbb{F})_{g,g'} \begin{bmatrix} \mathbf{P}_M^{g'} \\ \Phi_M^{g'} \end{bmatrix} - \sum_{g'=1}^{g-1} (\mathbb{M})_{g,g'} \begin{bmatrix} \mathbf{P}_{M+1}^{g'} \\ \Phi_{M+1}^{g'} \end{bmatrix} - \sum_{g'=g+1}^G (\mathbb{M})_{g,g'} \begin{bmatrix} \mathbf{P}_M^{g'} \\ \Phi_M^{g'} \end{bmatrix}.$$

These systems may be rewritten as

$$(\mathbb{A}^{g,g} + \mathbb{B}(\mathbb{T}^{g,g})^{-1}\mathbb{B}^T)\mathbf{P}_{M+1}^g = \mathbb{B}(\mathbb{T}^{g,g})^{-1}S_{M,\phi}^g - S_{M,\mathbf{P}}^g, \quad (13)$$

$$\Phi_{M+1}^g = (\mathbb{T}^{g,g})^{-1}(S_{M,\phi}^g - \mathbb{B}^T\mathbf{P}_{M+1}^g). \quad (14)$$

The eigenvalue is updated as follows

$$k_{M+1} = k_M \frac{(\mathbb{F}Z_{M+1})^T(\mathbb{F}Z_{M+1})}{(\mathbb{F}Z_M)^T(\mathbb{F}Z_{M+1})}. \quad (15)$$

We define the residual of the method at the M^{th} iteration by

$$\epsilon_M = \frac{\|k_{M+1}^{-1}\mathbb{F}Z_{M+1} - k_M^{-1}\mathbb{F}Z_M\|_{\ell^\infty}}{\|k_{M+1}^{-1}\mathbb{F}Z_{M+1}\|_{\ell^1}},$$

where the norms $\|\cdot\|_{\ell^\infty}$ and $\|\cdot\|_{\ell^1}$ are defined for all $Z \in \mathbb{R}^{\mathcal{N}}$, $\mathcal{N} > 0$, by $\|Z\|_{\ell^\infty} = \max_{1 \leq i \leq \mathcal{N}} |Z_i|$ and $\|Z\|_{\ell^1} = \sum_{i=1}^{\mathcal{N}} |Z_i|$. The convergence criteria is based on this residual.

In the absence of up-scattering (cf. Remark 3.2), the matrix \mathbb{M}_h is lower triangular by (energy group) block and the outer iteration corresponds to an exact resolution of the inverse power iteration.

4.2 Inner iteration

We apply an iterative scheme to solve (13): it is a Gauss-Seidel iteration over the directional blocks that is called alternative direction iteration. These iterations are called inner iterations. We consider now that the matrices $\mathbb{T}^{g,g}$, $1 \leq g \leq G$, are inexpensive to invert, i.e. that $(\mathbb{T}^{g,g})^{-1}$, $1 \leq g \leq G$, are available.

Remark 4.1. *In the case of a RTN finite element on rectangles ($d = 2$) or cuboids ($d = 3$), with well suited finite element degrees of freedom, the resulting matrices $\mathbb{T}^{g,g}$, $1 \leq g \leq G$, can be diagonal.*

Let us assume here that $d = 3$. The matrices $\mathbb{A}^{g,g'}$, $1 \leq g, g' \leq G$, and \mathbb{B} are (directional) block matrices

$$\begin{aligned} \mathbb{A}^{g,g'} &= ((\mathbb{A}_{x,x'}^{g,g'})_{1 \leq x, x' \leq d}), \\ \mathbb{B} &= ((\mathbb{B}_x)_{1 \leq x \leq d})^T. \end{aligned}$$

Remark 4.2. In the case of Cartesian meshes, $\mathbb{A}^{g,g'}$ is a (directional) block diagonal matrix.

We omit here the subscript M and the superscript g . Let \mathbf{P}_J be the approximation of \mathbf{P} at the inner iteration number J . For increasing $x = 1, \dots, d$, we solve the linear systems

$$(\mathbb{A}_{x,x}^{g,g} + \mathbb{B}_x(\mathbb{T}^{g,g})^{-1}(\mathbb{B}_x)^T)\mathbf{P}_{x,J} = S_{x,J},$$

where

$$S_{x,J} = Q - \sum_{x'=1}^{x-1} (\mathbb{A}_{x,x'}^{g,g} + \mathbb{B}_x(\mathbb{T}^{g,g})^{-1}\mathbb{B}_{x'})\mathbf{P}_{x',J+1} - \sum_{x'=x+1}^d (\mathbb{A}_{x,x'}^{g,g} + \mathbb{B}_x(\mathbb{T}^{g,g})^{-1}\mathbb{B}_{x'})\mathbf{P}_{x',J},$$

and Q is the right-hand side of (13).

4.3 Global description

We regroup in Algorithm 1 the global strategy implemented in the MINOS solver.

```

while not converged do
  Compute the source term  $Q_g$ 
   $Q_g = \sum_{g'=1}^G (\mathbb{F})_{g,g'} \begin{bmatrix} \mathbf{P}^{g'} \\ \Phi^{g'} \end{bmatrix}$ 
  for  $g = 1$  to  $G$  do
    update  $(\mathbb{M})_{g,g'}$  contribution from other energy groups,  $g' \neq g$ ,
     $Q_g = Q_g - \sum_{g' \neq g} (\mathbb{M})_{g,g'} \begin{bmatrix} \mathbf{P}^{g'} \\ \Phi^{g'} \end{bmatrix}$ 
    while not converged do
      for  $x = 1$  to  $d$  do
        Compute the source term  $Q_{g,x}$ 
         $Q_{g,x} = \mathbb{B}_x(\mathbb{T}^{g,g})^{-1}Q_\phi^g - \sum_{x' \neq x} (\mathbb{A}_{x,x'}^{g,g} + \mathbb{B}_x(\mathbb{T}^{g,g})^{-1}\mathbb{B}_{x'})\mathbf{P}_{x'}^g - Q_{\mathbf{p}_x}^g$ 
        Solve  $(\mathbb{A}_{x,x}^{g,g} + \mathbb{B}_x(\mathbb{T}^{g,g})^{-1}(\mathbb{B}_x)^T)\mathbf{P}_x^g = Q_{g,x}$ 
      end
       $\Phi^g = (\mathbb{T}^{g,g})^{-1}(Q_\phi^g - B^T \mathbf{P}^g)$ 
    end
  end
  update eigenvalue: (15)
end

```

Algorithm 1: The iterative strategy implemented in the MINOS solver

5 *A posteriori* error estimators for a mixed finite element discretization

In order to obtain *a posteriori* estimates, we use the so-called reconstruction of the discrete solution $\zeta_h = (\mathbf{p}_h, \phi_h)$ to (11). In what follows, we denote by $\tilde{\zeta}_h := \tilde{\zeta}_h(\zeta_h)$ a reconstruction, and by $\eta := \eta(\tilde{\zeta}_h)$

an estimator. Classically, our aim is to devise *reliable* and *efficient* estimators for the reconstructed error $\zeta - \tilde{\zeta}_h$, meaning that:

$$\begin{aligned} \|\zeta - \tilde{\zeta}_h\| &\leq \mathbf{C} \eta \quad (\text{reliability}) \\ \eta &\leq \mathbf{c} \|\zeta - \tilde{\zeta}_h\| \quad (\text{efficiency}) \end{aligned}$$

where \mathbf{C} and \mathbf{c} are generic constants, and $\|\cdot\|$ is some norm to measure the error. In what follows, we consider that

$$V = \underline{H}_0^1(\Omega), \text{ the original space of solutions, see (4),}$$

is the *default* space of scalar reconstructed fields. We also introduce the *broken spaces*

$$H^1(\mathcal{T}_h) = \{\psi \in L^2(\Omega) \mid \psi \in H^1(K), \forall K \in \mathcal{T}_h\}, \quad \mathbf{H}(\text{div}; \mathcal{T}_h) = \{\mathbf{q} \in \mathbf{L}^2(\Omega) \mid \mathbf{q} \in \mathbf{H}(\text{div}; K), \forall K \in \mathcal{T}_h\}.$$

A first approach has been suggested in [18, Chapter 8]. The reconstruction $\tilde{\zeta}_h = (\tilde{\mathbf{p}}_h, \tilde{\phi}_h)$ is defined as

$$\tilde{\mathbf{p}}_h = \mathbf{p}_h \in \mathbf{Q}_h \subset \mathbf{H}(\text{div}; \Omega), \quad \tilde{\phi}_h \in V.$$

Remark 5.1. For other boundary conditions, i.e. for a Neumann or Fourier boundary condition, the default space V of scalar reconstructed fields would be equal to $\underline{H}^1(\Omega)$.

5.1 Reconstruction of the discrete solution

In this section, we list some approaches to devise a reconstruction of the discrete solution (\mathbf{p}_h, ϕ_h) , here obtained with the RTN $_k$ finite element discretization, for $k \geq 0$. We refer to [7, Section 5.1] for a more exhaustive introduction of reconstruction approaches for RTN finite element spaces.

For illustrative purposes, we consider Cartesian meshes. Observe that the results presented in this section can be extended to the case of simplicial meshes [30]. Let us introduce some further notations, given such a mesh \mathcal{T}_h . The set of facets of \mathcal{T}_h is denoted \mathcal{F}_h , and it is split as $\mathcal{F}_h = \mathcal{F}_h^i \cup \mathcal{F}_h^e$, with \mathcal{F}_h^e (resp. \mathcal{F}_h^i) being the set of boundary facets (resp. interior facets). We denote by $\mathbb{Q}_k(\mathcal{T}_h)$ the space of piecewise polynomials of maximal degree k of each variable on each rectangle (or cuboid) $K \in \mathcal{T}_h$. We let \mathcal{V}_h^k be the set of interpolation points (or nodes) where the degrees of freedom of the V -conforming Lagrange Finite Element space of order k are defined. And, for a node $a \in \mathcal{V}_h^k$, we denote by \mathcal{T}_a the set of rectangles or cuboids K such that $a \in K$.

5.1.1 Average and average,+ reconstructions

To post-process, we consider first the averaging operator of the neutron flux $\mathcal{I}_{av} : \underline{\mathbb{Q}}_k(\mathcal{T}_h) \rightarrow \underline{\mathbb{Q}}_{k+1}(\mathcal{T}_h) \cap V$ such that

$$\forall \phi_h \in \underline{\mathbb{Q}}_k(\mathcal{T}_h), \forall a \in \mathcal{V}_h^{k+1}, \quad \mathcal{I}_{av}(\phi_h)(a) = \frac{1}{|\mathcal{T}_a|} \sum_{K \in \mathcal{T}_a} \phi_{h|K}(a).$$

The *average reconstruction* is

$$\tilde{\zeta}_{av,h} = (\mathbf{p}_h, \mathcal{I}_{av}(\phi_h)). \quad (16)$$

Similarly, we define another averaging operator $\mathcal{I}_{av,+} : \underline{\mathbb{Q}}_k(\mathcal{T}_h) \rightarrow \underline{\mathbb{Q}}_{k+2}(\mathcal{T}_h) \cap V$ such that

$$\forall \phi_h \in \underline{\mathbb{Q}}_k(\mathcal{T}_h), \forall a \in \mathcal{V}_h^{k+2}, \quad \mathcal{I}_{av,+}(\phi_h)(a) = \frac{1}{|\mathcal{T}_a|} \sum_{K \in \mathcal{T}_a} \phi_{h|K}(a).$$

The *average, + reconstruction* is

$$\tilde{\zeta}_{av,h} = (\mathbf{p}_h, \mathcal{I}_{av,+}(\phi_h)). \quad (17)$$

5.1.2 Post-processing reconstruction

We present here the approach proposed in [1], valid for any $k \geq 0$. It is shown there that the discrete solution ζ_h to (11), set in $\mathcal{X}_h = \mathbf{Q}_h \times L_h$, is also equal to the first argument of the solution of a hybrid formulation, where the constraint on the continuity of the normal trace of \mathbf{p}_h is relaxed. Let

$$\Lambda_h = \left\{ \lambda_h \in \underline{L^2}(\mathcal{F}_h^i) \mid \exists \mathbf{q}_h \in \mathbf{Q}_h, \lambda_h|_F = \mathbf{q}_h \cdot \mathbf{n}|_F, \forall F \in \mathcal{F}_h^i \right\},$$

be the space of the Lagrange multipliers and let $\tilde{\mathcal{X}}_h = \Pi_{K \in \mathcal{T}_h} \mathcal{X}_h(K)$ be the unconstrained approximation space with the RTN $_k$ local finite element spaces. By definition, \mathcal{X}_h is a strict subset of $\tilde{\mathcal{X}}_h$. The hybrid formulation is:

$$\left\{ \begin{array}{l} \text{Find } (\zeta_h, \lambda_h) \in \tilde{\mathcal{X}}_h \times \Lambda_h \text{ such that} \\ \forall (\xi_h, \mu_h) \in \tilde{\mathcal{X}}_h \times \Lambda_h, \quad c(\zeta_h, \xi_h) - \sum_{F \in \mathcal{F}_h^i} \int_F \lambda_h [\mathbf{q}_h \cdot \mathbf{n}] + \sum_{F \in \mathcal{F}_h^i} \int_F \mu_h [\mathbf{p}_h \cdot \mathbf{n}] = (S_f, \psi_h)_{0,\Omega}. \end{array} \right. \quad (18)$$

Let $\Pi_{M_h} : \tilde{\mathcal{X}}_h \times \Lambda_h \rightarrow M_h$ be the projection such that, given $(\zeta_h, \lambda_h) \in \tilde{\mathcal{X}}_h \times \Lambda_h$, $\hat{\phi}_h = \Pi_{M_h}(\zeta_h, \lambda_h)$ is governed by

$$\forall (\psi_h, \mu_h) \in L_h \times \Lambda_h, \quad (\mathbb{T}_e \hat{\phi}_h, \psi_h)_{0,\Omega} + \sum_{F \in \mathcal{F}_h^i} \int_F \hat{\phi}_h \mu_h = (\mathbb{T}_e \phi_h, \psi_h)_{0,\Omega} + \sum_{F \in \mathcal{F}_h^i} \int_F \lambda_h \mu_h.$$

See footnote¹ for a possible choice of space M_h .

In the field of neutronics, the post-processing is defined in [15] by $\mathcal{I}_{\text{RTN}}^2 : \tilde{\mathcal{X}}_h \times \Lambda_h \rightarrow \underline{\mathbb{Q}_{k+2}(\mathcal{T}_h)} \cap V$ such that

$$\forall (\zeta_h, \lambda_h) \in \tilde{\mathcal{X}}_h \times \Lambda_h, \quad \forall a \in \mathcal{V}_h^{k+2}, \quad \mathcal{I}_{\text{RTN}}^2(\zeta_h, \lambda_h)(a) = \frac{1}{|\mathcal{T}_a|} \sum_{K \in \mathcal{T}_a} (\Pi_{M_h}(\zeta_h, \lambda_h))|_K(a).$$

The chosen *post-processing reconstruction* is finally

$$\tilde{\zeta}_{\text{RTN},h} = (\mathbf{p}_h, \mathcal{I}_{\text{RTN}}^2(\zeta_h, \lambda_h)). \quad (19)$$

¹ In dimension 3, the space M_h is defined as $M_h = \Pi_{K \in \mathcal{T}_h} M_h(K)$, where for all $K \in \mathcal{T}_h$,

$$M_h(K) = \underline{\mathbb{Q}_{k+2,k,k}(K)} \oplus \underline{\mathbb{Q}_{k,k+2,k}(K)} \oplus \underline{\mathbb{Q}_{k,k,k+2}(K)}$$

See [1] for the definition of *ad hoc* finite-dimensional spaces M_h for other families and types of elements.

5.2 A posteriori error estimate

Let us define

$$\begin{aligned} d_S(\zeta, \xi) &= (\mathbb{D}^{-1} \mathbf{p}, \mathbf{q})_{0,\Omega} + (\mathbb{T}_e \phi, \psi)_{0,\Omega} \\ d(\zeta, \xi) &= d_S(\zeta, \xi) + (\psi, \operatorname{div} \mathbf{p})_{0,\Omega} - (\phi, \operatorname{div} \mathbf{q})_{0,\Omega} = c(\zeta, (-\mathbf{q}, \psi)). \end{aligned}$$

The definition is extended to piecewise smooth fields on \mathcal{T}_h by replacing \int_{Ω} by $\sum_{K \in \mathcal{T}_h} \int_K$.

Extending the approach in [7], we propose to use a weighted $\mathbf{H}(\operatorname{div}; \mathcal{T}_h) \times \underline{L}^2(\Omega)$ norm. One may define

$$\delta_{e,K}^{max} = \max_{g \in \mathcal{I}_G} \sup_K ((\mathbb{T}_e)_{g,g}), \quad \delta_{e,K}^{min} = \min_{g \in \mathcal{I}_G} \inf_K ((\mathbb{T}_e)_{g,g}); \quad D_K^{max} = \max_{g \in \mathcal{I}_G} \sup_K (D^g), \quad D_K^{min} = \min_{g \in \mathcal{I}_G} \inf_K (D^g).$$

We define the following norm on \mathcal{X} , for all $\zeta \in \mathcal{X}$,

$$\|\zeta\|_{S,MG}^2 = \sum_{K \in \mathcal{T}_h} \|\mathbb{D}^{-1/2} \mathbf{p}\|_{0,K}^2 + \|\delta_e^{1/2} \phi\|_{0,K}^2 + \sum_{K \in \mathcal{T}_h} h_K^2 (D_K^{min})^{-1} \|(\operatorname{div} \mathbf{p})\|_{0,K}^2,$$

where δ_e the diagonal part of \mathbb{T}_e , and $\delta_e^{1/2}$ is its square root. By design, the diagonal entries of δ_e are all strictly positive: $(\phi, \psi) \mapsto (\delta_e \phi, \psi)_{0,K}$ defines an inner product in $\underline{L}^2(K)$, so one can measure $\phi|_K$ in the associated norm $\phi \mapsto ((\delta_e \phi, \phi)_{0,K})^{1/2}$, and finally $((\delta_e \phi, \phi)_{0,K})^{1/2} = \|\delta_e^{1/2} \phi\|_{0,K}$.

Remark 5.2. *By contrast, in general, \mathbb{T}_e is not a symmetric matrix, so $(\phi, \psi) \mapsto (\mathbb{T}_e \phi, \psi)_{0,K}$ does not define an inner product. On the other hand, since \mathbb{T}_e is strictly diagonal dominant with small off-diagonal entries (cf. remark 3.1), it is expected that $(\delta_e \phi, \phi)_{0,K}$ is an accurate approximation of $(\mathbb{T}_e \phi, \phi)_{0,K}$.*

We introduce the following \mathcal{X}_K -local norm, for all $\zeta \in \mathcal{X}$,

$$|\zeta|_{+,K} = \sup_{\xi \in \mathcal{X}_K, \|\xi\|_{S,MG} \leq 1} d(\zeta, \xi), \quad (20)$$

with $N(K) = \{K' \in \mathcal{T}_h \mid \dim_H(\partial K' \cap \partial K) = d - 1\}$, where \dim_H is the Hausdorff dimension, and

$$\mathcal{X}_K = \{\zeta = (\mathbf{p}, \phi) \in \mathcal{X}, \operatorname{Supp}(\phi) \subset K, \operatorname{Supp}(\mathbf{p}) \subset N(K)\}.$$

Observe that the norm $\|\cdot\|_{S,MG}$ measures elements of \mathcal{X} in $\mathbf{H}(\operatorname{div}, \mathcal{T}_h) \times \underline{L}^2(\Omega)$ norm. This corresponds precisely to the energy norm (cf. [18, Chapter 8]).

Let ζ and ζ_h be respectively the solution to (6) and (11). Let $\tilde{\zeta}_h = (\mathbf{p}_h, \tilde{\phi}_h)$ be a reconstruction of ζ_h in $\mathbf{Q}_h \times V$. For any $K \in \mathcal{T}_h$, we define the residual estimators

$$\eta_{r,K} = \|\delta_e^{-1/2} (S_f - \operatorname{div} \mathbf{p}_h - \mathbb{T}_e \tilde{\phi}_h)\|_{0,K}, \quad (21)$$

the flux estimator

$$\eta_{f,K} = \|\mathbb{D}^{1/2} (\mathbb{D}^{-1} \mathbf{p}_h + \mathbf{grad} \tilde{\phi}_h)\|_{0,K}. \quad (22)$$

Then it stands for all $K \in \mathcal{T}_h$,

$$|\zeta - \tilde{\zeta}_h|_{+,K} \leq \left(\eta_{r,K}^2 + \sum_{K' \in N(K)} \eta_{f,K'}^2 \right)^{1/2}. \quad (23)$$

In order to state the next estimate on the local efficiency of the *a posteriori* error estimators, we will assume that the entries of the matrices \mathbb{T}_e and \mathbb{D} are piecewise polynomials on \mathcal{T}_h and $S_f \in L_h$. In addition, we suppose that $\tilde{\phi}_h$ is piecewise polynomial on \mathcal{T}_h . The former assumption can be restrictive in the sense that it imposes a constraint on the model. On the other hand, the latter assumption only depends on the choice of the reconstruction. Let $K \in \mathcal{T}_h$ and let $\eta_{r,K}$ and $\eta_{f,K}$ be the residual estimators respectively given by (21) and (22). We have the following estimate

$$\eta_{r,K} \leq \mathbf{c} \left(\frac{\delta_{e,K}^{max}}{\delta_{e,K}^{min}} \right)^{1/2} |\zeta - \tilde{\zeta}_h|_{+,K}, \quad (24)$$

$$\eta_{f,K} \leq \mathbf{C} \left(\frac{D_K^{max}}{D_K^{min}} \right)^{1/2} |\zeta - \tilde{\zeta}_h|_{+,K}, \quad (25)$$

where \mathbf{c} and \mathbf{C} are constants which depend only on the polynomial degree of S_f , \mathbb{T}_e , d , and the shape-regularity parameter κ_K , with the $|\cdot|_{+,K}$ norm defined as in (20).

The proof of these results for the multi-group diffusion equation is an extension of the study for the diffusion mono-group equation proposed in [7, Section 5.2.3]. For the sake of brevity, details of the numerical analysis for the multigroup diffusion equation will be given in a companion paper.

6 Adaptive mesh refinement

In this Section, we recall a classical definition of an AMR strategy. This iterative process is divided into four modules as presented in Figure 1, where $\varepsilon_{\text{AMR}} > 0$ is a user-defined parameter

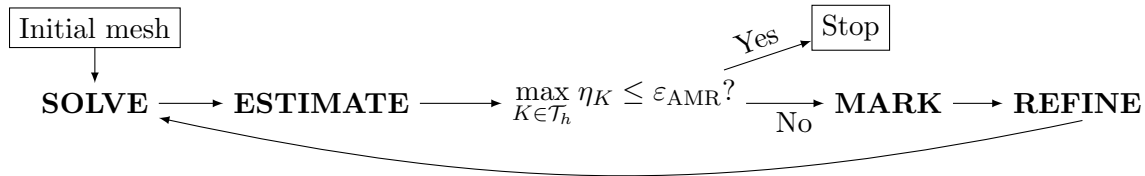


Figure 1: Description of the AMR process.

6.1 SOLVE module

For the source problem, the **SOLVE** module amounts to solving the discrete source problem (11). In the case of the criticality problem, it corresponds to solving the discrete eigenvalue problem (12).

6.2 ESTIMATE module

In the **ESTIMATE** module, the local error indicator η_K is computed on each element $K \in \mathcal{T}_h$. Using the *a posteriori* error estimate (23), this error indicator is defined by

$$\eta_K := \left(\eta_{r,K}^2 + \sum_{K' \in N(K)} \eta_{f,K'}^2 \right)^{1/2}.$$

6.3 MARK module

The purpose of the **MARK** module is to select a set of elements with large error: then, these elements are refined. In other words, the marking strategy consists in selecting a set S of elements of minimal cardinality such that one has

$$\eta(S) \simeq \theta \eta(\mathcal{T}_h), \quad \text{where} \quad \eta(S) := \left(\sum_{K \in S} \eta_K^2 \right)^{1/2}, \quad \text{resp.} \quad \eta(\mathcal{T}_h) := \left(\sum_{K \in \mathcal{T}_h} \eta_K^2 \right)^{1/2}$$

and $\theta > 0$ is a user-defined parameter. According to [7, Section 6], an efficient strategy which preserves the Cartesian structure of the mesh is the *direction* marker strategy. One selects for each direction \mathbf{e}_x , $x = 1, \dots, d$, the smallest set of lines L_x along that direction such that $\eta(L_x) \geq \theta \eta(\mathcal{T}_h)$. The resulting selected set is $\cup_{x=1, \dots, d} L_x$.

6.4 REFINE module

The **REFINE** module refines the mesh \mathcal{T}_h if the stopping criterion $\max_{K \in \mathcal{T}_h} \eta_K \leq \varepsilon_{\text{AMR}}$ is not reached.

7 Numerical illustration

This section is dedicated to the numerical experiments where we apply the adaptive mesh refinement (AMR) described in Section 6 to industrial benchmark test cases. In fact, we compare the AMR process with respect to the choice of the flux reconstruction (involved in the definition of the total estimator):

- (1) average;
- (2) average,+;
- (3) post-processing.

In particular, for the same threshold number $\varepsilon_{\text{AMR}} > 0$, the total number of elements denoted by N_h is shown to illustrate the efficiency of the AMR strategy with different reconstruction methods. In this section, we apply a RTN₀ finite element discretization and we consider the uniform Cartesian mesh with the mesh size $5\text{cm} \times 5\text{cm} \times 5\text{cm}$ as the initial mesh for the AMR process, where the dimensions of Ω in the x, y, z -directions are in the order of $140\text{cm} - 320\text{cm}$, see below. We slightly modify the boundary conditions of the benchmark test cases; we impose the zero-flux boundary condition instead of the vacuum boundary condition in our test cases.

7.1 Takeda Model 2

We aim to focus on the small Fast Breeder Reactor (FBR) (Model 2) of the 3D benchmark proposed by Takeda et al. in [27] with dimensions of 140cm \times 140cm \times 150cm which includes a core region, radial and axial blankets, and a control rod region. The reactor core geometry (quarter reactor core) is shown in Figure 2. The reactor core calculation is performed in 4 energy groups with the cross sections given in A. In this problem, we would like to consider the following two cases:

- Case 1: the control rod is withdrawn ;
- Case 2: the control rod is half-inserted.

The so-called reference multiplication factors, computed on a uniform 2.5cm \times 2.5cm \times 2.5cm mesh with RTN₂ elements are given in Table 1. According to Tables 2 and 3, the AMR performs better if the estimators are computed with the average reconstruction than with the average,+ reconstruction. This implies that using average operator with high order polynomial does not improve the accuracy of the estimator. On the other hand, the post-processing reconstruction reduces dramatically the total number of elements in the AMR process compared to the average reconstruction. Therefore, the post-processing reconstruction really improves the accuracy of the total estimator. Moreover, it is worth pointing out that the result depends strongly on the value of the parameter θ as shown in Tables 4 and 5.

Although the $k_{\text{eff},h}$ obtained with the AMR processes of the average and average,+ reconstruction are closer to the reference multiplication factor, these processes are significantly less efficient with respect to the stopping criterion ε_{AMR} . In addition, we observe that if one carries out more iterations of the AMR process of the post-processing reconstruction, one recovers a more accurate multiplication factor with fewer mesh elements. We refer to the values in italics in Table 2 where an error of 8 pcm (or $8 \cdot 10^{-5}$) is reached for $N_h \simeq 1.2 \cdot 10^6$, whereas $N_h > 2.3 \cdot 10^7$ is needed for the other two methods to reach an error of 9 pcm (or $9 \cdot 10^{-5}$) at best; similar observations are made with the values in italics in Table 3.

Figure 3 illustrates the total estimator on the initial mesh for both cases. This figure clearly shows that the total estimator is large only at the rod positions for the test with half inserted control rod (case 2) while it is large mainly on the interface between the Core and Radial Blanket for the test case where the control rod is fully withdrawn (case 1).

Test case	Case 1	Case 2
k_{eff}	0.96361	0.94923

Table 1: The reference value of k_{eff} for Model 2

7.2 Takeda Model 3

The third model of the benchmark proposed by Takeda et al. is an axially heterogeneous FBR with dimensions of 320cm \times 320cm \times 180cm. The geometry of the reactor core is shown in Figures 4 and 5. In particular, this reactor core is composed of internal blanket, core region, radial blanket, axial blanket, control rod region, radial reflector, axial reflector and empty matrix. The reactor core calculation is also performed in 4 groups with cross sections given in A and the following three cases are considered:

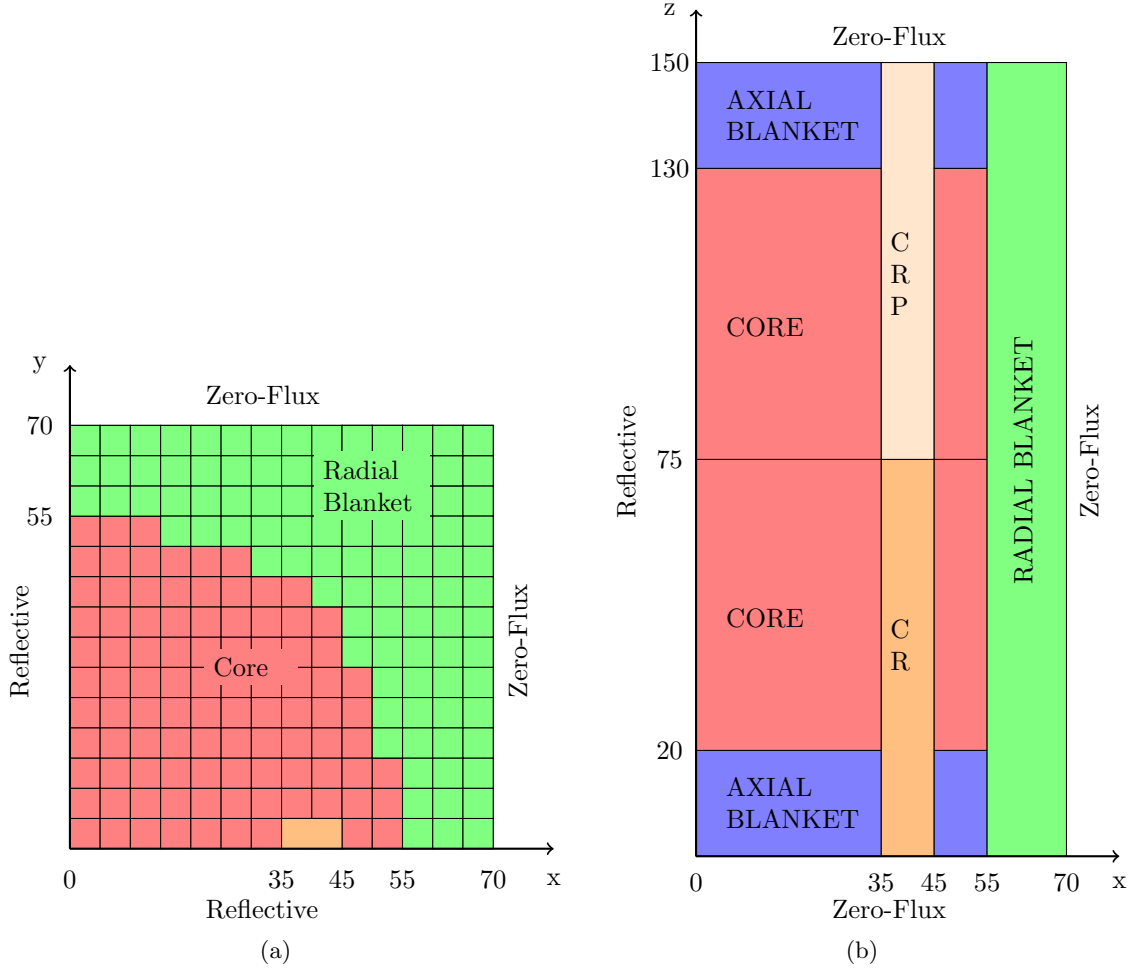


Figure 2: Small FBR geometry

It	Average			Average,+			Post-processing		
	N_h	$\max_{K \in \mathcal{T}_h} \eta_K$	$k_{\text{eff},h}$	N_h	$\max_{K \in \mathcal{T}_h} \eta_K$	$k_{\text{eff},h}$	N_h	$\max_{K \in \mathcal{T}_h} \eta_K$	$k_{\text{eff},h}$
0	23 520	0.40015	0.96405	23 520	0.49119	0.96405	23 520	0.08151	0.96405
1	62 320	0.28764	0.96407	62 320	0.35711	0.96406	62 361	0.06078	0.96407
2	165 996	0.23558	0.96410	157 092	0.35114	0.96410	188 328	0.03626	0.96412
3	473 550	0.13855	0.96413	450 000	0.19158	0.96413	564 570	0.01318	0.96397
4	921 600	0.07268	0.96374	902 400	0.11024	0.96374	1 168 128	0.00993	0.96369
5	2 315 163	0.05644	0.96373	2 143 464	0.10117	0.96373			
6				6 289 630	0.05894	0.96370			

Table 2: Takeda Model 2 case 1 with $\theta = 0.5$ and $\varepsilon_{\text{AMR}} = 0.06$

It	Average			Average, +			Post-processing		
	N_h	$\max_{K \in \mathcal{T}_h} \eta_K$	$k_{\text{eff},h}$	N_h	$\max_{K \in \mathcal{T}_h} \eta_K$	$k_{\text{eff},h}$	N_h	$\max_{K \in \mathcal{T}_h} \eta_K$	$k_{\text{eff},h}$
0	23 520	1.67384	0.95016	23 520	1.10946	0.95016	23 520	0.45990	0.95016
1	59 163	0.53247	0.94981	59 163	0.740026	0.94981	59 204	0.22517	0.95000
2	159 848	0.24804	0.94976	148 257	0.31938	0.94972	175 230	0.06047	0.94983
3	466 792	0.25122	0.94973	414 720	0.223137	0.94973	536 640	0.02665	0.94974
4	975 200	0.12797	0.94938	920 000	0.20069	0.94939	<i>1 036 800</i>	<i>0.01847</i>	<i>0.94938</i>
5	2 446 272	0.07737	0.94935	2 221 560	0.10953	0.94936	<i>2 561 424</i>	<i>0.01288</i>	<i>0.94937</i>
6	7 777 908	0.05029	0.94931	6 771 984	0.07823	0.94933	<i>8 294 400</i>	<i>0.00966</i>	<i>0.94927</i>
7				9 676 800	0.07822	0.94926			
8				21 546 096	0.040907	0.94926			

Table 3: Takeda Model 2 case 2 with $\theta = 0.5$ and $\varepsilon_{\text{AMR}} = 0.06$

It	$\theta = 0.4$			$\theta = 0.45$			$\theta = 0.6$		
	N_h	$\max_{K \in \mathcal{T}_h} \eta_K$	$k_{\text{eff},h}$	N_h	$\max_{K \in \mathcal{T}_h} \eta_K$	$k_{\text{eff},h}$	N_h	$\max_{K \in \mathcal{T}_h} \eta_K$	$k_{\text{eff},h}$
0	23 520	0.08151	0.96405	23 520	0.08151	0.96405	23 520	0.08151	0.96405
1	53 391	0.06504	0.96406	57 760	0.06074	0.96406	75 768	0.05246	0.96409
2	130 000	0.04628	0.96411	157 304	0.04493	0.96411			

Table 4: Takeda Model 2 case 1 with post-processing reconstruction and $\varepsilon_{\text{AMR}} = 0.06$

It	$\theta = 0.4$			$\theta = 0.45$			$\theta = 0.6$		
	N_h	$\max_{K \in \mathcal{T}_h} \eta_K$	$k_{\text{eff},h}$	N_h	$\max_{K \in \mathcal{T}_h} \eta_K$	$k_{\text{eff},h}$	N_h	$\max_{K \in \mathcal{T}_h} \eta_K$	$k_{\text{eff},h}$
0	23 520	0.45990	0.95016	23 520	0.45990	0.95016	23 520	0.45990	0.95016
1	50 544	0.24341	0.94999	54 760	0.22516	0.95000	72 283	0.20503	0.94994
2	119 808	0.06190	0.94982	143 055	0.06189	0.94983	253 890	0.05535	0.94984
3	291 200	0.05325	0.94983	383 116	0.04903	0.94982			

Table 5: Takeda Model 2 case 2 with post-processing reconstruction and $\varepsilon_{\text{AMR}} = 0.06$

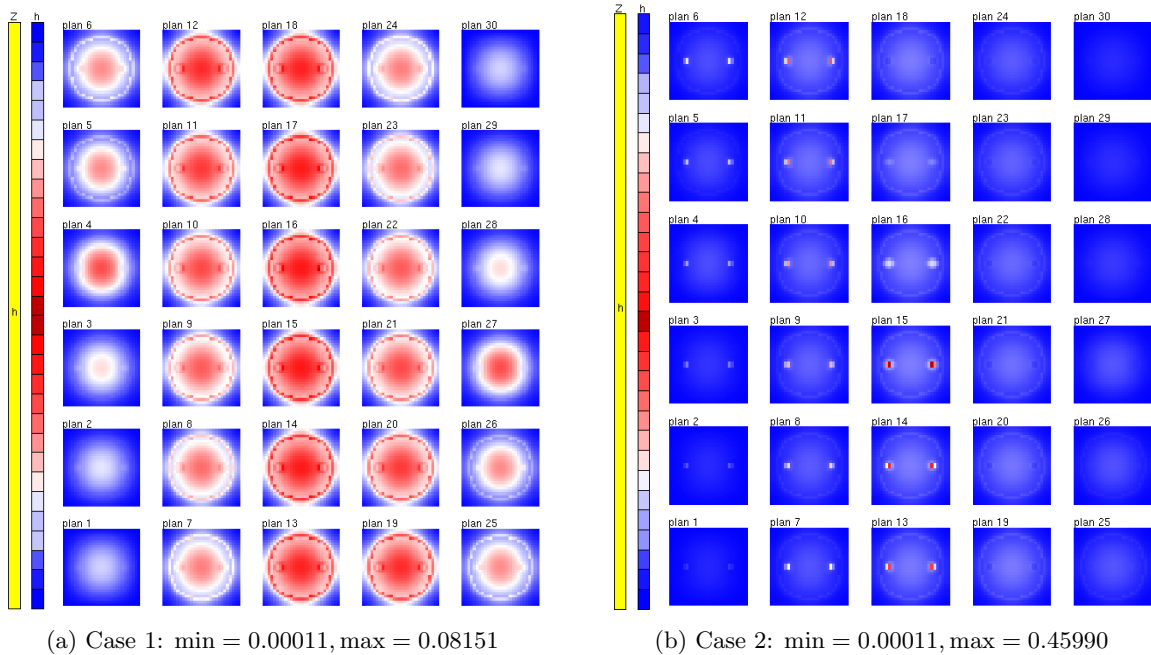


Figure 3: Total estimator on the initial mesh for Model 2 - Post-processing reconstruction

- Case 1: the control rods are inserted ;
- Case 2: the control rods are withdrawn ;
- Case 3: the control rods are replaced with core and/or blanket cells.

The so-called reference multiplication factors, computed on a uniform $2.5\text{cm} \times 2.5\text{cm} \times 2.5\text{cm}$ mesh with RTN_2 elements are given in Table 6. Since the average,+ reconstruction behaves similarly as discussed in the Takeda model 2, we only focus on the average and the post-processing reconstructions in this benchmark test case. Tables 7, 8 and 9 show that the AMR process with the estimator computed with the post-processing reconstruction performs much better than with the average reconstruction. Figure 6 illustrates the behavior of the total estimator on the initial mesh for the model 3. As can be seen, it is large only at the control rods for the case 1, while it is large mainly at both the control rod positions and the interface among materials for case 2 and finally it is large only on the interface among materials for case 3. Moreover, Table 10 shows some initial refined meshes of the AMR process with the estimator computed with the post-processing reconstruction for all test cases, which are in good agreement with the behavior of the total estimator.

Test case	Case 1	Case 2	Case 3
k_{eff}	0.96259	0.99333	1.01562

Table 6: The reference value of k_{eff} for Model 3

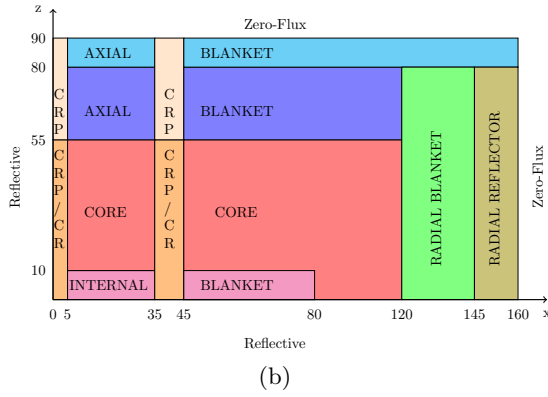
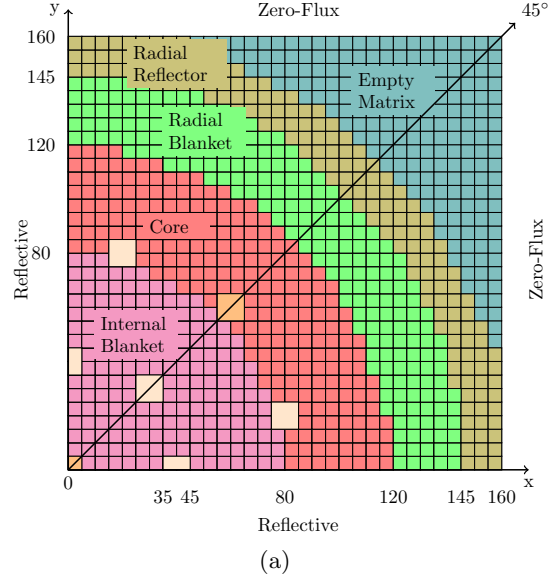
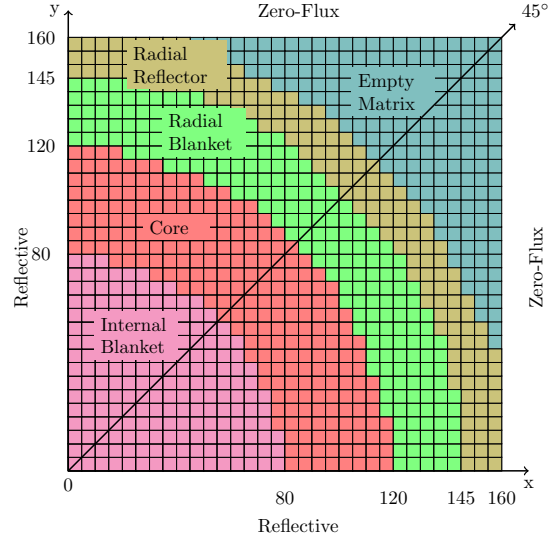


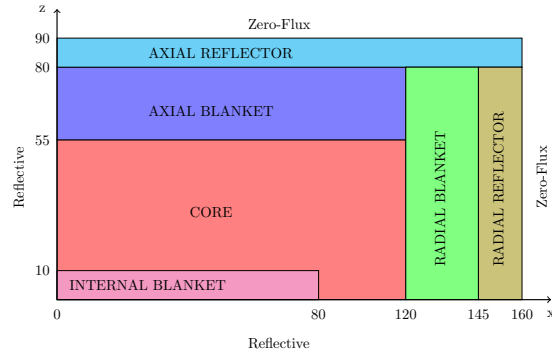
Figure 4: Configuration of Model 3 case 1 and case 2

It	Average			Post-processing		
	N_h	$\max_{K \in \mathcal{T}_h} \eta_K$	$k_{\text{eff},h}$	N_h	$\max_{K \in \mathcal{T}_h} \eta_K$	$k_{\text{eff},h}$
0	23 520	1.49448	0.96356	23 520	0.33723	0.96356
1	338 688	0.41143	0.96303	354 025	0.08414	0.96307
2	901 552	0.26117	0.96284	962 948	0.05274	0.96290
3	2 420 640	0.10432	0.96282			
4	5 573 056	0.07457	0.96270			
5	14 149 440	0.03725	0.96265			

Table 7: Takeda Model 3 case 1 with $\theta = 0.5$ and $\varepsilon_{\text{AMR}} = 0.06$



(a)



(b)

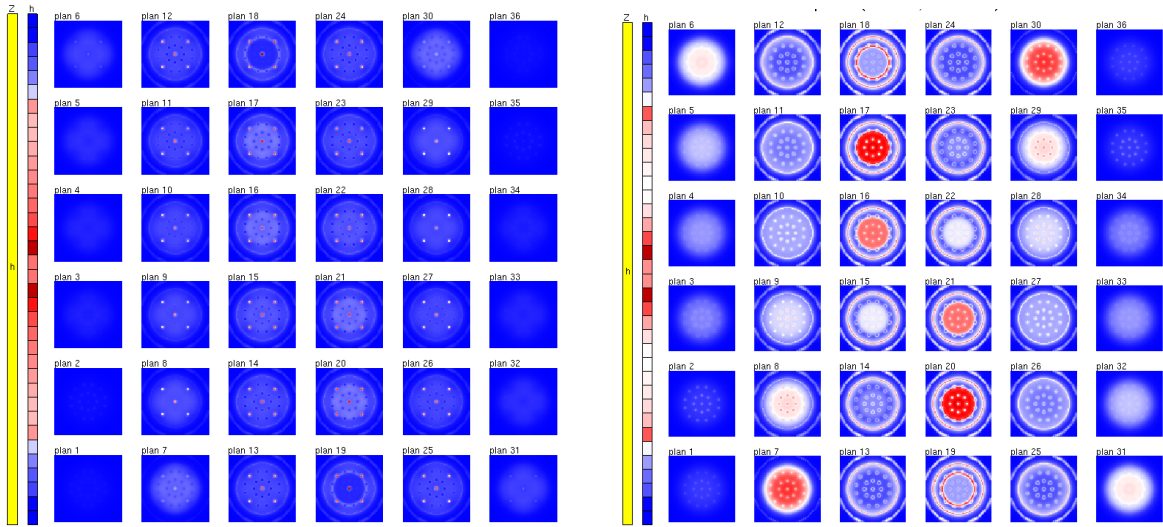
Figure 5: Configuration of Model 3 case 3

It	Average			Post-processing		
	N_h	$\max_{K \in \mathcal{T}_h} \eta_K$	$k_{\text{eff},h}$	N_h	$\max_{K \in \mathcal{T}_h} \eta_K$	$k_{\text{eff},h}$
0	23 520	0.26708	0.99348	23 520	0.07390	0.99348
1	354 025	0.28711	0.99348	370 881	0.05321	0.99352
2	948 787	0.17333	0.99347			
3	2 568 384	0.10356	0.99346			
4	5 537 792	0.04697	0.99336			

Table 8: Takeda Model 3 case 2 with $\theta = 0.5$ and $\varepsilon_{\text{AMR}} = 0.06$

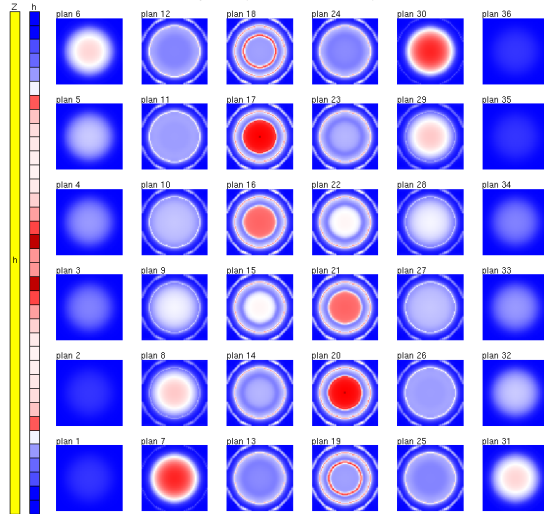
It	Average			Post-processing		
	N_h	$\max_{K \in \mathcal{T}_h} \eta_K$	$k_{\text{eff},h}$	N_h	$\max_{K \in \mathcal{T}_h} \eta_K$	$k_{\text{eff},h}$
0	23 520	0.27265	1.01571	23 520	0.07585	1.01571
1	354 025	0.18980	1.01573	37 0881	0.05058	1.01577
2	934 626	0.16462	1.01574			
3	2 511 936	0.09597	1.01573			
4	5 537 792	0.04556	1.01564			

Table 9: Takeda Model 3 case 3 with $\theta = 0.5$ and $\varepsilon_{\text{AMR}} = 0.06$



(a) Case 1: $\min = 3.28 \times 10^{-6}$, $\max = 0.335723$

(b) Case 2: $\min = 4.10 \times 10^{-6}$, $\max = 0.07390$



(c) Case 3: $\min = 5.27 \times 10^{-6}$, $\max = 0.07585$

Figure 6: Total estimator on the initial mesh for Model 3 - Post-processing reconstruction

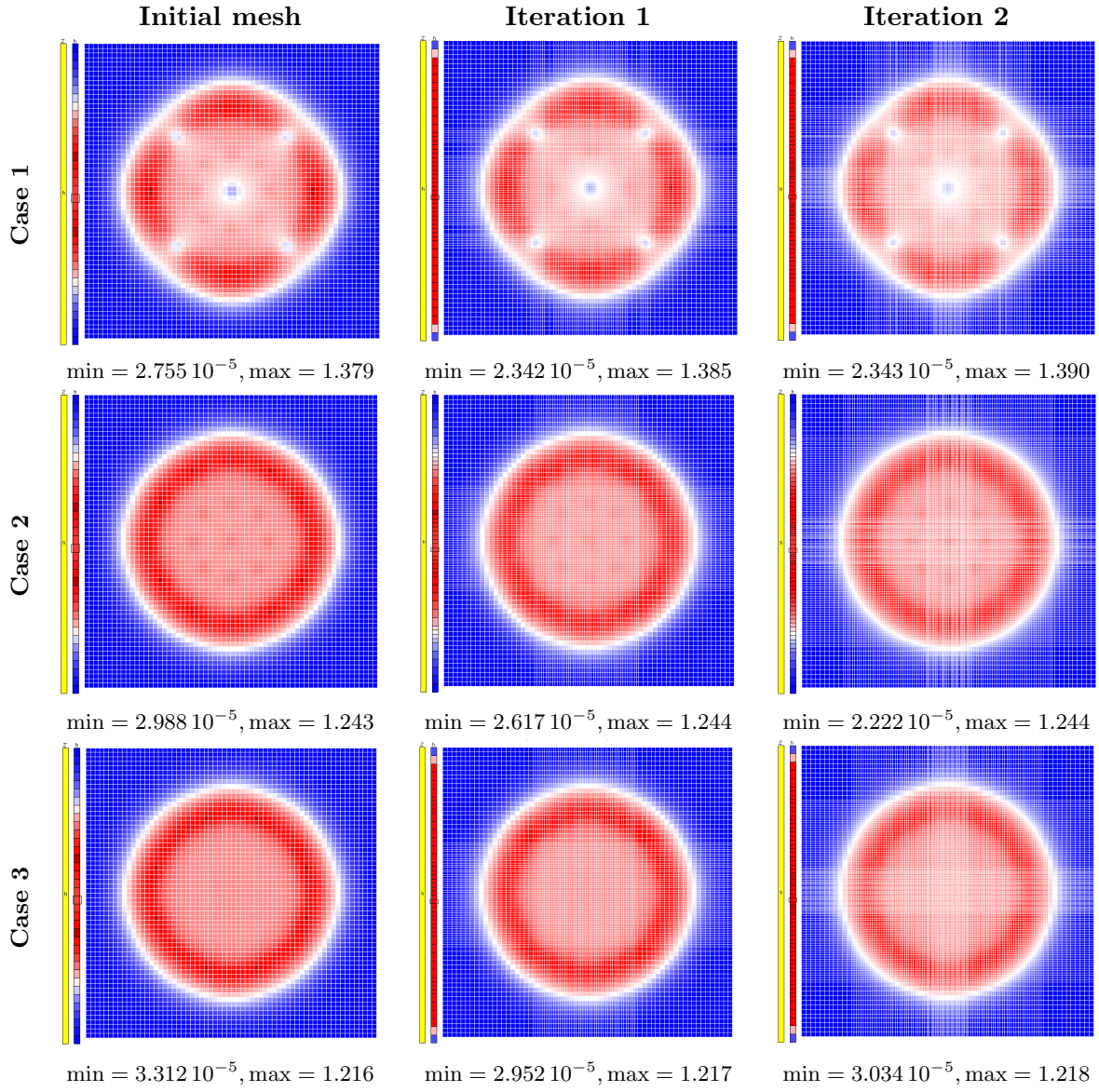


Table 10: (Refined meshes) Flux of the second energy group of model 3 at the central axial plane - Post-processing reconstruction

8 Conclusion

In this manuscript, we applied an AMR strategy to the mixed finite element discretization of the multigroup neutron diffusion equations. This approach is based on *a posteriori* estimators that are both reliable and locally efficient.

We use a refinement strategy that preserves the Cartesian structure of the mesh. The potential of the approach is demonstrated on specific benchmarks coming from reactor physics application. We compare AMR processes with various *a posteriori* estimators. The post-processing reconstruction is shown to be more efficient than the average and average,+ reconstructions. We observe numerically that the AMR strategy is sensitive to the choice of the threshold parameter.

In a companion paper, we will consider a more general model, widely used for nuclear core simulations, the multigroup simplified transport problem, for which we will provide *a posteriori* estimators. These estimators will be proven to be reliable and locally efficient.

Acknowledgements

APOLLO3[®] is a registered trademark of CEA. We gratefully acknowledge EDF and Framatome for their long-term partnership and their support.

A Energy groups and cross-sections for the Takeda benchmark

For the sake of completeness, we detail in this appendix the energy groups and cross sections of the materials in the Takeda benchmarks.

Group	Energy range (eV)		Fission Spectrum χ
	Upper	Lower	
1	$1.00000 \cdot 10^7$	$1.35340 \cdot 10^6$	0.583319
2	$1.35340 \cdot 10^6$	$8.65170 \cdot 10^4$	0.405450
3	$8.65170 \cdot 10^4$	$9.61120 \cdot 10^2$	0.011231
4	$9.61120 \cdot 10^2$	$1.00000 \cdot 10^{-5}$	0.

Table 11: Energy range and Fission Spectrum

Core				
Group	1	2	3	4
Σ_t	$1.14568 \cdot 10^{-1}$	$2.05177 \cdot 10^{-1}$	$3.29381 \cdot 10^{-1}$	$3.89810 \cdot 10^{-1}$
$\nu\Sigma_f$	$2.06063 \cdot 10^{-2}$	$6.10571 \cdot 10^{-3}$	$6.91403 \cdot 10^{-3}$	$2.60689 \cdot 10^{-2}$
$\Sigma_{s,0}^{g \rightarrow 1}$	$7.04326 \cdot 10^{-2}$	0.	0.	0.
$\Sigma_{s,0}^{g \rightarrow 2}$	$3.47967 \cdot 10^{-2}$	$1.95443 \cdot 10^{-1}$	0.	0.
$\Sigma_{s,0}^{g \rightarrow 3}$	$1.88282 \cdot 10^{-3}$	$6.20863 \cdot 10^{-3}$	$3.20586 \cdot 10^{-1}$	0.
$\Sigma_{s,0}^{g \rightarrow 4}$	0.	$7.07208 \cdot 10^{-7}$	$9.92975 \cdot 10^{-4}$	$3.62360 \cdot 10^{-1}$

Table 12: Cross sections in the Core region

Radial and Inner Blanket				
Group	1	2	3	4
Σ_t	$1.19648 \cdot 10^{-1}$	$2.42195 \cdot 10^{-1}$	$3.56476 \cdot 10^{-1}$	$3.79433 \cdot 10^{-1}$
$\nu\Sigma_f$	$1.89496 \cdot 10^{-2}$	$1.75265 \cdot 10^{-4}$	$2.06978 \cdot 10^{-4}$	$1.13451 \cdot 10^{-3}$
$\Sigma_{s,0}^{g \rightarrow 1}$	$6.91158 \cdot 10^{-2}$	0.	0.	0.
$\Sigma_{s,0}^{g \rightarrow 2}$	$4.04132 \cdot 10^{-2}$	$2.30626 \cdot 10^{-1}$	0.	0.
$\Sigma_{s,0}^{g \rightarrow 3}$	$2.68621 \cdot 10^{-3}$	$9.57027 \cdot 10^{-3}$	$3.48414 \cdot 10^{-1}$	0.
$\Sigma_{s,0}^{g \rightarrow 4}$	0.	$1.99571 \cdot 10^{-7}$	$1.27195 \cdot 10^{-3}$	$3.63631 \cdot 10^{-1}$

Table 13: Cross sections in the Radial and Inner Blanket regions

Radial Reflector				
Group	1	2	3	4
Σ_t	$1.71748 \cdot 10^{-1}$	$2.17826 \cdot 10^{-1}$	$4.47761 \cdot 10^{-1}$	$7.95199 \cdot 10^{-1}$
$\nu\Sigma_f$	0.	0.	0.	0.
$\Sigma_{s,0}^{g \rightarrow 1}$	$1.23352 \cdot 10^{-1}$	0.	0.	0.
$\Sigma_{s,0}^{g \rightarrow 2}$	$4.61307 \cdot 10^{-2}$	$2.11064 \cdot 10^{-1}$	0.	0.
$\Sigma_{s,0}^{g \rightarrow 3}$	$1.13217 \cdot 10^{-3}$	$6.27100 \cdot 10^{-3}$	$4.43045 \cdot 10^{-1}$	0.
$\Sigma_{s,0}^{g \rightarrow 4}$	0.	$1.03831 \cdot 10^{-6}$	$2.77126 \cdot 10^{-3}$	$7.89497 \cdot 10^{-1}$

Table 14: Cross sections in the Radial Reflector region

Axial Blanket				
Group	1	2	3	4
Σ_t	$1.16493 \cdot 10^{-1}$	$2.20521 \cdot 10^{-1}$	$3.44544 \cdot 10^{-1}$	$3.88356 \cdot 10^{-1}$
$\nu\Sigma_f$	$1.31770 \cdot 10^{-2}$	$1.26026 \cdot 10^{-4}$	$1.52380 \cdot 10^{-4}$	$7.87302 \cdot 10^{-4}$
$\Sigma_{s,0}^{g \rightarrow 1}$	$7.16044 \cdot 10^{-2}$	0.	0.	0.
$\Sigma_{s,0}^{g \rightarrow 2}$	$3.73170 \cdot 10^{-2}$	$2.10436 \cdot 10^{-1}$	0.	0.
$\Sigma_{s,0}^{g \rightarrow 3}$	$2.21707 \cdot 10^{-3}$	$8.59855 \cdot 10^{-3}$	$3.37506 \cdot 10^{-1}$	0.
$\Sigma_{s,0}^{g \rightarrow 4}$	0.	$6.68299 \cdot 10^{-7}$	$1.68530 \cdot 10^{-3}$	$3.74886 \cdot 10^{-1}$

Table 15: Cross sections in the Axial Blanket region

Axial Reflector				
Group	1	2	3	4
Σ_t	$1.65612 \cdot 10^{-1}$	$1.66866 \cdot 10^{-1}$	$2.68633 \cdot 10^{-1}$	$8.34911 \cdot 10^{-1}$
$\nu\Sigma_f$	0.	0.	0.	0.
$\Sigma_{s,0}^{g \rightarrow 1}$	$1.15653 \cdot 10^{-1}$	0.	0.	0.
$\Sigma_{s,0}^{g \rightarrow 2}$	$4.84731 \cdot 10^{-2}$	$1.60818 \cdot 10^{-1}$	0.	0.
$\Sigma_{s,0}^{g \rightarrow 3}$	$8.46495 \cdot 10^{-4}$	$5.64096 \cdot 10^{-3}$	$2.65011 \cdot 10^{-1}$	0.
$\Sigma_{s,0}^{g \rightarrow 4}$	0.	$6.57573 \cdot 10^{-7}$	$2.41755 \cdot 10^{-3}$	$8.30547 \cdot 10^{-1}$

Table 16: Cross sections in the Axial Reflector region

Empty Matrix				
Group	1	2	3	4
Σ_t	$1.36985 \cdot 10^{-2}$	$1.69037 \cdot 10^{-2}$	$3.12271 \cdot 10^{-2}$	$6.29537 \cdot 10^{-2}$
$\nu\Sigma_f$	0.	0.	0.	0.
$\Sigma_{s,0}^{g \rightarrow 1}$	$9.57999 \cdot 10^{-3}$	0.	0.	0.
$\Sigma_{s,0}^{g \rightarrow 2}$	$3.95552 \cdot 10^{-3}$	$1.64740 \cdot 10^{-2}$	0.	0.
$\Sigma_{s,0}^{g \rightarrow 3}$	$8.80428 \cdot 10^{-3}$	$3.91394 \cdot 10^{-4}$	$3.09104 \cdot 10^{-2}$	0.
$\Sigma_{s,0}^{g \rightarrow 4}$	0.	$7.72254 \cdot 10^{-8}$	$1.77293 \cdot 10^{-4}$	$6.24581 \cdot 10^{-2}$

Table 17: Cross sections in the Empty Matrix region

Group	Control Rod			
	1	2	3	4
Σ_t	$1.84333 \cdot 10^{-1}$	$3.66121 \cdot 10^{-1}$	$6.15527 \cdot 10^{-1}$	1.09486
$\nu\Sigma_f$	0.	0.	0.	0.
$\Sigma_{s,0}^{g \rightarrow 1}$	$1.34373 \cdot 10^{-1}$	0.	0.	0.
$\Sigma_{s,0}^{g \rightarrow 2}$	$4.37775 \cdot 10^{-2}$	$3.18582 \cdot 10^{-1}$	0.	0.
$\Sigma_{s,0}^{g \rightarrow 3}$	$2.06054 \cdot 10^{-4}$	$2.98432 \cdot 10^{-2}$	$5.19591 \cdot 10^{-1}$	0.
$\Sigma_{s,0}^{g \rightarrow 4}$	0.	$8.71188 \cdot 10^{-7}$	$7.66209 \cdot 10^{-3}$	$6.18265 \cdot 10^{-1}$

Table 18: Cross sections in the (empty) Control Rod regions

Group	Na Filled CRP			
	1	2	3	4
Σ_t	$6.58979 \cdot 10^{-2}$	$1.09810 \cdot 10^{-1}$	$1.86765 \cdot 10^{-1}$	$2.09933 \cdot 10^{-1}$
$\nu\Sigma_f$	0.	0.	0.	0.
$\Sigma_{s,0}^{g \rightarrow 1}$	$4.74407 \cdot 10^{-2}$	0.	0.	0.
$\Sigma_{s,0}^{g \rightarrow 2}$	$1.76894 \cdot 10^{-2}$	$1.06142 \cdot 10^{-1}$	0.	0.
$\Sigma_{s,0}^{g \rightarrow 3}$	$4.57012 \cdot 10^{-4}$	$3.55466 \cdot 10^{-3}$	$1.85304 \cdot 10^{-1}$	0.
$\Sigma_{s,0}^{g \rightarrow 4}$	0.	$1.77599 \cdot 10^{-7}$	$1.01280 \cdot 10^{-3}$	$2.08858 \cdot 10^{-1}$

Table 19: Cross sections in the sodium filled Control Rod regions

References

- [1] T. ARBOGAST AND Z. CHEN, *On the implementation of mixed methods as nonconforming methods for second-order elliptic problems*, Math. Comp., 64 (1995), pp. 943–972.
- [2] I. BABUŠKA AND M. SURI, *The p and h - p versions of the finite element method, basic principles and properties*, SIAM Rev., 36 (1994), pp. 578–632.
- [3] I. BABUŠKA, B. SZABO, AND I. KATZ, *The p -version of the finite element method*, SIAM J. Numer. Anal., 18 (1981), pp. 515–545.
- [4] A.-M. BAUDRON AND J.-J. LAUTARD, *MINOS: A Simplified P_N solver for core calculation*, Nuclear Science and Engineering, 155 (2007), pp. 250–263.
- [5] D. BOFFI, F. BREZZI, AND M. FORTIN, *Mixed and hybrid finite element methods and applications*, Springer-Verlag, 2013.
- [6] W. CAO, W. HUANG, AND R. RUSSELL, *An r -adaptive finite element method based upon moving mesh PDEs*, J. Comput. Phys., 149 (1999), pp. 221–244.
- [7] P. CIARLET, JR., M. H. DO, AND F. MADIOT, *A posteriori error estimates for mixed finite element discretizations of the neutron diffusion equations*, ESAIM: M2AN, 57 (2023), pp. 1–27.
- [8] P. CIARLET, JR., E. JAMELOT, AND F. D. KPADONOU, *Domain decomposition methods for the diffusion equation with low-regularity solution*, Comput. Math. Applic., 74 (2017), pp. 2369–2384.
- [9] W. DAHMEN, F. GRUBER, AND O. MULA, *An adaptive nested source term iteration for radiative transfer equations*, Mathematics of Computation, 89 (2020), pp. 1605–1646.
- [10] W. DAHMEN AND O. MULA, *Accuracy controlled schemes for the eigenvalue problem of the radiative transfer equation*, 2023.
- [11] P. DANIEL, A. ERN, I. SMEARS, AND M. VOHRALÍK, *An adaptive hp -refinement strategy with computable guaranteed bound on the error reduction factor*, Comput. Math. Applic., 76 (2018), pp. 967–983.
- [12] R. DAUTRAY AND J.-L. LIONS, *Mathematical Analysis and Numerical Methods for Science and Technology: Volume 6 Evolution Problems II*, Springer Science & Business Media, 2012.
- [13] M.-H. DO, F. MADIOT, AND P. CIARLET, JR., *Adaptive solution of the neutron diffusion equation with heterogeneous coefficients using the mixed finite element method on structured meshes*, EPJ Web Conf., (2021).
- [14] J. J. DUDERSTADT AND L. J. HAMILTON, *Nuclear reactor analysis*, John Wiley & Sons, Inc., 1976.
- [15] F. FÉVOTTE, *Une méthode de post-traitement des éléments finis de Raviart-Thomas appliquée à la neutronique*. CMAP Seminar, Palaiseau, May, 2019.
- [16] D. FOURNIER, R. LE TELLIER, AND C. SUTEAU, *Analysis of an a posteriori error estimator for the transport equation with S_N and discontinuous Galerkin discretizations*, Annals of Nuclear Energy, 38 (2011), pp. 221–231.

- [17] C. FÜHRER AND G. KANSCHAT, *A posteriori error control in radiative transfer*, Computing, 58 (1997), pp. 317–334.
- [18] L. GIRET, *Non-conforming domain decomposition for the multigroup neutron SP_N equations*, PhD thesis, Université Paris Saclay, 2018.
- [19] E. JAMELOT AND P. CIARLET, JR., *Fast non-overlapping Schwarz domain decomposition methods for solving the neutron diffusion equation*, J. Comput. Phys., 241 (2013), pp. 445–463.
- [20] J. LANG, W. CAO, W. HUANG, AND R. RUSSELL, *A two-dimensional moving finite element method with local refinement based on a posteriori error estimates*, Appl. Numer. Math., 46 (2003), pp. 75–94.
- [21] D. LATHOUWERS, *Goal-oriented spatial adaptivity for the S_N equations on unstructured triangular meshes*, Annals of Nuclear Energy, 38 (2011), pp. 1373–1381.
- [22] ———, *Spatially adaptive eigenvalue estimation for the S_N equations on unstructured triangular meshes*, Annals of Nuclear Energy, 38 (2011), pp. 1867–1876.
- [23] P. MOSCA, L. BOURHRARA, A. CALLOO, A. GAMMICCHIA, F. GOUBILOUD, L. MAO, F. MADIOT, F. MALOUCH, E. MASIELLO, F. MOREAU, S. SANTANDREA, D. SCIANNANDRONE, I. ZMIJAREVIC, E. Y. GARCIA-CERVANTES, G. VALOCCHI, J. F. VIDAL, F. DAMIAN, P. LAURENT, A. WILLIEN, A. BRIGHENTI, L. GRAZIANO, AND B. VEZZONI, *Apollo3®: Overview of the new code capabilities for reactor physics analysis*, Nuclear Science and Engineering, 0 (2024), pp. 1–14.
- [24] J.-C. NÉDÉLEC, *Mixed finite elements in \mathbb{R}^3* , Numer. Math., 35 (1980), pp. 315–341.
- [25] A. OWENS, J. KÓPHÁZI, J. WELCH, AND M. EATON, *Energy dependent mesh adaptivity of discontinuous isogeometric discrete ordinate methods with dual weighted residual error estimators*, Journal of Computational Physics, 335 (2017), pp. 352–386.
- [26] P.-A. RAVIART AND J.-M. THOMAS, *A mixed finite element method for second order elliptic problems*, in Mathematical aspects of finite element methods, vol. 606 of Lecture Notes in Mathematics, Springer, 1977, pp. 292–315.
- [27] T. TAKEDA AND H. IKEDA, *3-D neutron transport benchmarks*, Journal of Nuclear Science and Technology, 28 (1991), pp. 656–669.
- [28] R. VARGA, *Matrix iterative analysis*, (1962).
- [29] R. VERFÜRTH, *A posteriori error estimation and adaptive mesh-refinement techniques*, J. Comput. Appl. Math., 50 (1994), pp. 67–83.
- [30] M. VOHRALÍK, *Unified primal formulation-based a priori and a posteriori error analysis of mixed finite element methods*, Math. Comp., 79 (2010), pp. 2001–2032.